Final Draft

of the original manuscript

Macchi, J.; Gaudez, S.; Geandier, G.; Teixeira, J.; Denis, S.; Bonnet, F.; Allain, S.:

Dislocation densities in a low-carbon steel during martensite transformation determined by in situ high energy X-Ray diffraction.

In: Materials Science and Engineering: A. Vol. 800 (2021) 140249.

First published online by Elsevier: 19.09.2020

https://dx.doi.org/10.1016/j.msea.2020.140249

Dislocation densities in a low-carbon steel during martensite transformation determined by In situ High Energy X-Ray Diffraction

Authors

Macchi Juan[1], Gaudez Steve[1], Geandier Guillaume[1], Teixeira Julien[1], Denis Sabine[1], Bonnet Frédéric[2], Allain Sébastien Y.P[1]

[1] Institut Jean Lamour, UMR 7198 CNRS Université de Lorraine, Campus ARTEM Nancy, France

[2] ArcelorMittal Research SA, APRC, Voie Romaine, BP 30320, 57283 Maizières les Metz, France

Keywords: Steel ; Martensite ; Synchrotron ; X-ray analysis; Dislocation ; Mechanical behavior

Corresponding author:

Macchi, Juan

juan.macchi@univ-lorraine.fr

Tel.: +33 03 72 74 26 87

Postal address: Campus Artem, 2 allée André Guinier, 54011 Nancy

Abstract

The evolution of the dislocation densities in martensite and in austenite during the quench of a low-carbon (0.215 wt.% C) steel is investigated in situ by the mean of a High Energy X-Ray Diffraction experiment on a synchrotron beamline. The line configuration offers an excellent time resolution well adapted to the studied martensitic transformation kinetics. The mean density of dislocations in martensite increases as the transformation proceeds confirming that dislocations are not homogeneously distributed between the laths in agreement with some recent post-mortem observations. The resulting spatial distribution of dislocations and the associated strain-hardening support the views assuming that lath martensite is a heterogeneous microstructure and behaves as a "multiphase" aggregate. In austenite, the increase in dislocation densities is even more significant meaning that austenite in martensite is also a hard phase, contradicting some recent theories attributing to films of retained austenite a major role in the plasticity of martensite.

Graphical Abstract

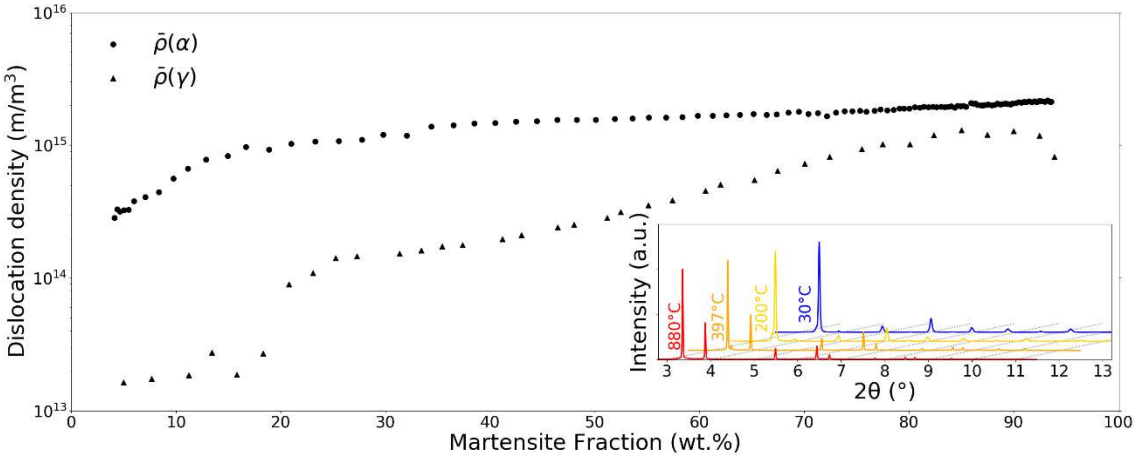

Highlights

- In situ High Energy X-Ray Diffraction experiments have been conducted during a quenching experiment to determine at the same time the progress of the martensitic transformation and the densities of dislocations in both phases (martensite and austenite).
- Post-processing the history of the measurements in both phase during the transformation allows to isolate the dislocation density in the newly formed martensitic laths. This provides the complete distribution of dislocation densities in the final microstructure.
- The distribution of local yield strength resulting from the dislocations is found to be a first order contribution to explain the mechanical behavior of martensite.

- Very high dislocation densities are also found in the residual austenite pointing out that this latter should be probably as hard as martensite laths.

Introduction

Although lath martensites are one of the key microstructure constituents of conventional steels, of hot-stamped boron-bearing steels and also of several 3rd generation multi-phased steels for automotive construction [1], the correlation between their mechanical behavior and their specific hierarchical microstructure is not completely established yet. A major reason is that most of the studies have considered martensite as an homogeneous structure. Recent works in this field have tried to highlight that martensite microstructures are in fact dispersed in terms of size, residual stresses, defects and composition and behave like a multiphase aggregate [2–4]. These results sustain thus the micromechanical approach considering martensite as a continuum composite material (CCA) [2,3] proposed by the present authors already in 2012 and assuming a distribution of local yield strengths at the microstructure scale. Since then, this interpretation has been supported either by local mechanical measurements or by direct microstructure observations.

Some authors have found a wide dispersion of the mechanical properties between different martensite laths thanks to nanohardness investigations. Li et al. [5] showed that the nanohardness within the martensite studied can vary between 5 GPa and 11 GPa. It has been observed that the smaller blocks (aggregate of laths with low angle misorientation) have a higher hardness in [6] with an average nanohardness of about 5.5 GPa for the large blocks and 6.9 GPa in the small blocks with a width estimated by

77 Electron Backscattered Diffraction (EBSD) equal to 6 and 3.5 μm respectively. He et
78 al. [7] studied ferritic microstructures (ferrite, lower and upper bainite, and martensite)
79 highlighting a significantly wider scattering in the martensite results. In addition a high
80 heterogeneity in the deformation of this phase was reported in [8] by digital image
81 correlation based on successive EBSD cartographies taken during the test. The
82 heterogeneity was reported to increase with deformation indicating strain localization
83 and indicating a huge dispersion in the local yield strengths of the laths.
84 These local dispersions and the resulting composite behavior are related to the
85 martensite transformation itself, which is essentially displacive and athermal. Very few
86 studies have been dedicated to the formation of microstructure heterogeneities in
87 martensite. Starting from post mortem observations, Morsdorf et al. [9] have analyzed
88 how the martensite microstructure appears progressively. The study shows the presence
89 of a wide dispersion of thickness, with thin laths (from ≈50 to ≈500 nm) and coarse lath,
90 up to ≈3.5μm. A quantitative analysis by atom probe tomography in thin and coarse
91 laths reveals that carbon segregation is more intense in the coarse laths than in the thin
92 ones. Nanohardness characterization presented in the same work shows that the thinner
93 laths were ≈10% harder than the coarse ones. It suggests that the first martensite
94 blocks/lath to appear will be the largest, the most segregated and the softest. On the
95 contrary, the last structures to form will be the hardest domains of the microstructure
96 [9]. Similar conclusions were drawn by Badinier et al. [10,11].
97 To the authors' best knowledge, Christien et al. [12] were the only group to study in situ
98 the evolution of the mean dislocation density during the martensite transformation in
99 both martensite and austenite. The study was conducted by neutron diffraction and the
100 studied steel was a carbon-free stainless steel permitting long acquisition time (1 pattern

every 2 mins). Results showed that the higher the martensite phase fraction, the higher the mean dislocation densities in both phases.

The present work consists also in the detailed characterization of the evolution of mean dislocation density in both martensite and austenite phases in situ during the transformation. We have addressed the challenge to follow these evolutions in a low carbon steel in which martensitic transformation is faster and can be accompanied by self-tempering mechanisms. A set-up with an excellent time resolution suitable for these particular steels and transformation kinetics (1 pattern every 0.1s) was used. Moreover, an analysis to determine in the final microstructure the associated spatial dispersion of local hardening due to these dislocations was developed. This new insight permits to go farther in the understanding of the mechanical properties of this heterogeneous phase.

Material and methods

An industrial low-carbon alloyed steel, provided by ArcelorMittal Maizières Research Center, France, with a composition Fe-0.215C-0.25Si-1.82Mn-0.18Cr wt.% was investigated. The steel was received after the cold-rolling stage (1.5 mm thickness) and samples were machined by 10 mm x 4 mm x 1.5 mm plates. No surface preparation was performed.

High Energy X-ray diffraction (HEXRD) experiments were performed in situ at the Deutsche-Elektronen-Synchrotron (DESY, PETRA-III) P07 beam line with a monochromatic beam with an energy of 100 keV (λ=0.012398 nm) allowing to work in transmission mode. The association with a fast 2D Perkin-Elmer detector enabled high acquisition rates (10 Hz) needed to study fast processes on bulk samples (400 x 400 µm beam size by 1.5 mm thickness) with a sufficient time resolution, as it is the case of the martensitic transformation in low carbon steels. The detector was positioned about 1.5 m behind the sample, giving access to full Debye-Scherrer rings with a maximum 2θ angle of 8° (5 Debye Scherrer rings per phase).

Martensitic quench treatment was performed with a modified Bähr DIL805 A/D dilatometer available on the beam line. The heat treatment used to investigate the martensite transformation consists of a heating at 20 °C/s up to 880 °C, followed by an isothermal holding during 180 s and finally of a fast cooling by argon gas blowing (aiming at a cooling rate of 50°C/s) down to the room temperature. The austenitization heat treatment leads to a mean prior austenite grain size of 6.5 µm. This value has been determined by Prior Austenite Grain reconstruction using Decrypt® software on the basis of EBSD cartographies (results not shown here). For the studied cooling, 500

136 diffraction patterns have been acquired between the Ms temperature (394°C) of the
137 alloy and the room temperature.
138 The 2D diffraction patterns produced during the experiments were integrated circularly
139 using pyFAI python library [13]. The deduced 1D diffractograms (Intensity vs 2θ) were
140 analyzed with a Rietveld refinement procedure using pseudo-Voigt functions to
141 reproduce diffraction peaks. The Rietveld method here has served to obtain the phase
142 fractions with an uncertainty of ±1% (absolute value) during the martensitic
143 transformation. According to 1D diagrams, two phases were considered during the
144 analysis: martensite with a body centered tetragonal structure (I/4 mmm) and austenite
145 with a cubic face centered structure (Fm-3m). No carbide (transition iron carbides
146 and/or cementite) resulting from martensite self-tempering was detected during the
147 quench by HEXRD, even if such configurations is known to enable their detection if
148 present in low amount [14]. Three experiments have been conducted in order to ensure
149 the repeatability.
150 For simplicity, and to avoid redundancy, only one experiment is presented and discussed
151 in the present paper. The other experiments show strong similarity with the one
152 presented here, and the same conclusions would be extracted from each investigation.
153 Nevertheless, the results of each individual experiments are available in the
154 supplementary data.
155
156 Since the pioneer works of Williamson & Hall [15], it is well known that dislocations
157 present in polycrystals will affect the width of their diffraction peaks. The higher the
158 dislocation density (resp. the lower the crystallite size), the larger the peak width [16].
159 The Rietveld method does not permit to determine properly the Full Width Half

160 Maximum (FWHM(2θ)) of each diffraction peaks as it is only a mean description of a
161 full line profile. In fact, the FWHM in Fullprof is based on the Caglioti et al.'s theory
162 [17] which required the refinement of three parameters per phase to describe the mean
163 FWHM for each of its peak. This description does not permit to account in particular for
164 the respective crystallographic anisotropy of the phases as suggested by Ungar et al.
165 [18].
166 Besides the Rietveld refinement of the full diffractograms, a separate refinement has
167 thus been conducted peak by peak using Pearson VII functions in order to obtain the
168 individual FWHM and angular position of the phase diffraction peaks. The instrumental
169 contribution to the peaks broadening was measured with a silicon powder and
170 subtracted from the measured FWHM by considering a square additive law [19]. The
171 instrumental contribution was considered constant during the proposed experiments
172 accounting for the stability of the beam during each experiment and considering that the
173 only parameter that changes is the temperature of the sample, no movement has been
174 made even on the sample or the detector.
175 While a tetragonal cell was used for the Rietveld refinement, it was not possible to
176 model each peak individually considering tetragonality with one Pearson VII function
177 per diffraction plane family. The diffraction peaks were then fitted with a single
178 symmetric Pearson VII function. This introduces an over estimation in the dislocation
179 density as the peaks will be slightly larger than expected due to the tetragonal lattice. At
180 the end of the martensitic transformation, one diffractogram was analyzed both by a
181 single function per diffraction peak and by one Pearson VII function per diffraction
182 plane families considering tetragonality imposing the difference between positions due
183 to the c/a determined by the Rietveld refinement (1.006). For clarity, in the case of the

peak (200) the diffraction plane families are (hk0) and (00l) and the effect of the tetragonality (1.006) in the experimental set-up produces a difference of 0.03° 2θ between both families. The dislocation density found in the second case was only 12% lower than only considering one function by peak. The error introduced considering a single peak instead of two for the fitting procedure is low in regard to the experimental uncertainties for the low carbon steel studied and would not modify the tendencies found and conclusions extracted.

From the instrumently-corrected FWHMs, the dislocation densities in martensite and in austenite for each studied diffraction patterns were estimated by the modified Williamson-Hall method (mWH), introduced by Ungár et al. [18]. This method imposes a contrast factor for each refracting plane family considering the anisotropy of the material [20]. Under the assumption that the only feature introducing broadening in the materials reflections are the dislocations and crystallite sizes, the peak broadening can be described by the following equation:

$$\Delta K = \mathfrak{z}/D + (((\pi M b^2)/2)^{1/2} * \bar{\rho}^{1/2}) * K * \bar{C}_{hkl}^{1/2} + OK^2 \bar{C}_{hkl} \qquad (1)$$

where ΔK=FWHM(θ)*2cos(θ))/λ , K is the norm of the scattering vector defined by K=2sin(θ)/λ, D is the crystallite size, M is a parameter depending on the dislocation density, b is the Burgers vector, $\bar{\rho}$ is the mean dislocation density and $\bar{C}_{hkl}$ is the average contrast factor of dislocations for the specific reflection. $OK^2\ \bar{C}_{hkl}$ is a higher order term with no meaning established [21], where O is much smaller than the coefficient before $K\bar{C}_{hkl}$, and it is not considered here [22]. For the present work $\mathfrak{z}$ was set equal to 0.9 as done in [15] and b to 2.5 10^{-10}m (ca. 2.49 10^{-10}m and 2.517 10^{-10}m respectively for the ferrite and the austenite) for both phases analyzed. M is a dimensionless parameter linked to the outer cut-off radius of the dislocations and the dislocation arrangement

208 inside the phase, this parameter can be evaluated with the Warren-Averbach method. In
209 the present study this parameter was considered constant during the thermal treatment.
210 While it can vary [19], it is set at 2.2 considering the average value from [23].
211 The dislocation contrast factor for each reflection ($\bar{C}_{hkl}$) is taken from ANIZC software
212 [24] which gives the theoretical contrast factor for screw and for edge type dislocations.
213 It accounts from the type of lattice (considered as cubic here), the second order elastic
214 constants and reflections [24]. The slip systems considered for edge dislocation are
215 <111> {110} and <110> {111} respectively for the body-centered and face-centered-
216 cubic phases. The dislocation lines considered for screw are <111> and <110>
217 respectively for the body-centered and face-centered-cubic. As the elastic constants
218 (C_{11}, C_{12} and C_{44}) vary with the temperature [25–27], the dislocation contrast factors
219 vary as well. The dislocation contrast factors for screw and edge type dislocations are
220 considered as temperature dependent and have been calculated using the values in the
221 literature for ferrite [25–27]. For austenite, they have been considered constant due to
222 the lack of available data [28]. Many models propose a description of isotropic elastic
223 constants but the data considering the elastic anisotropy of the lattice are rare. However,
224 as the phases are considered separately in this second post-treatment, the error made in
225 austenite has not effect on the results for martensite
226 Table 1 shows the dislocation contrast factor calculated at room temperature for both
227 martensite and austenite considering a ratio of 50% edge and 50% screw type
228 dislocations as [19]. The contrast factor evolutions with temperature for martensite were
229 calculated up to 700°C and fitted with a second order polynomial function ($aT^2 + bT + c$
230 with T in K). For the {200} reflection fitted parameters are a=1.73 10^{-7}, b=4.854 10^{-5}

and c=0.277 while for {211}{220}{321} they are a=2.266 10^{-8}, b=7.042 10^{-7} and c=0.1408 for the considered proportion of dislocation types.

An estimation of the error introduces by neglecting the elastic constants thermal dependence was performed on the martensite phase at 350 °C. The dislocation density was found 7% lower than accounting for the thermal dependence. The influence of this sensitivity in thus limited in the studied temperature range. Based on this result, we could expect similar results for austenite in the investigated temperature range (between Ms down to RT).

Table 1: Dislocation contrast factors at room temperature for both ferrite and austenite considering a ratio of 50% edge and 50% screw type dislocations.

Ferrite	{200}	{211}	{220}	{321}
$\bar{C}_{hkl}$	0.278	0.141	0.141	0.141
Austenite	{200}	{220}	{311}	{420}
$\bar{C}_{hkl}$	0.299	0.148	0.204	0.202

In order to estimate an error introduced by the possible texture of the steel and the experimental scattering, one 2D image (Debye Scherrer rings) from the end of the quench was integrated circularly each degree yielding to 360 1D diagrams. Each diagram was analyzed with the mWH procedure. The calculations (results not shown here) show that 95% of the dislocations densities calculated, for both martensite and austenite phases, where in between the mean value and ±22.5% (i.e. the dispersion from the mean value for two standard deviations (95%) was lower than ±22.5%).

Results:

The cooling curve of the most representative in situ experiment is presented in Figure 1(a) with the corresponding dilatometric signal. The first evidence of martensitic transformation is observed on the dilatometric curve due to the transformation strain from austenite to martensite. In addition, as martensitic transformation is by nature an exothermic reaction, it affects the thermal evolution. The apparent martensite start temperature (Ms) was found equal to 394±4°C by the analysis of 3 dilatometric curves and applying the offset method proposed by Yang and Bhadeshia [29]. This temperature corresponds also to a deviation in the temperature evolution (sudden change in slope). Nevertheless, in the studied condition, the transformation appears to be sluggish at the beginning as only 5% of martensite is formed at 360°C. These points will be clarified and discussed later at the light of the XRD data.

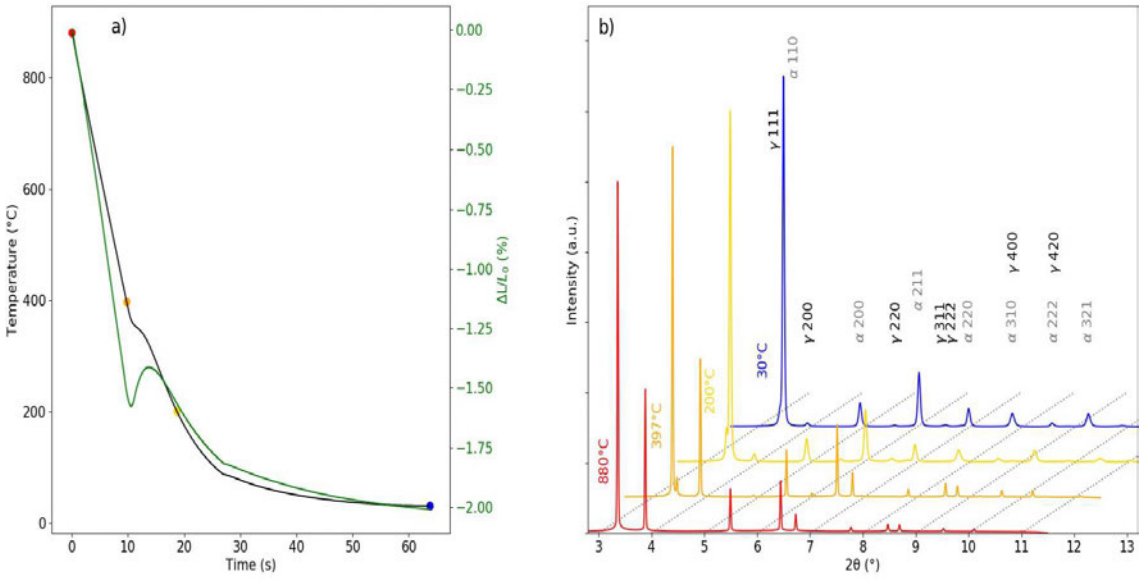

Figure 1: a) Cooling and dilatometric curves as function of time and b) 1D diffractograms recorded during the HEXRD in situ experiment corresponding to the temperatures highlighted on the cooling curve, respectively 880, 394 (Ms), 200 and 30 °C. The deformation and the time were set at 0 at the end of the austenitization stage.

Some selected 1D diffractograms of the same experiment are presented in Figure 1(b) They correspond to the conditions highlighted by dots in Figure 1(a). The same color code has been followed. The respective reflections of austenite and martensite are indicated (α standing for ferrite and martensite and γ for austenite). Along the cooling sequence, the alloy is first fully austenitic at 880°C. At the apparent Ms temperature (394°C), the diffraction pattern shows already the presence of small fraction of ferritic phase (<5wt.%). This fraction is attributed to a ferritic or a bainitic transformation prior to the martensitic transformation. At 200°C and at RT, the alloy is mainly martensitic. The martensite phase fraction measured at room temperature is 94 wt.% and is similar between the experiments, meaning that 6 wt.% of austenite is retained at RT.

Figure 2 presents the progress of the martensitic transformation, i.e. the martensite weight fraction evolution during the quench as a function of the temperature by XRD. The transformation kinetics obtained by dilatometry have been plotted from 0 (before the start of the transformation) to 100 (end of detected transformation) in the same figure. The values measured by XRD encompass all ferritic phases (possible ferrite transformation before Ms and martensitic transformation). Both methods show that the transformation kinetics is initially not following a kinetics as it could be predicted by Koistinen and Marburger and then a rapid transformation is observed. The sudden increase in the transformation kinetics by the Rietveld analysis occurs around 365°C which is 32°C lower than the apparent Ms reported above. This second value agrees well with the theoretical Ms temperature of the investigated steel (369°C) accounting for the nominal steel composition and the prior austenite grain size (PAGS) [30,31]. This two steps transformation is common in industrial steels and is often explained by microsegregations or decarburized surface layer which affect the local transformation

start temperature [32,33]. As a consequence, there is a spatial and time distribution of the transformation progression. The transformation starts earlier in microstructure regions where the Ms is high (low C, low Mn, high PAGS) and later where Ms is lower. In the following, 365°C will be considered as the true Ms temperature of the alloy considering it represents better the value of the alloy mean composition.

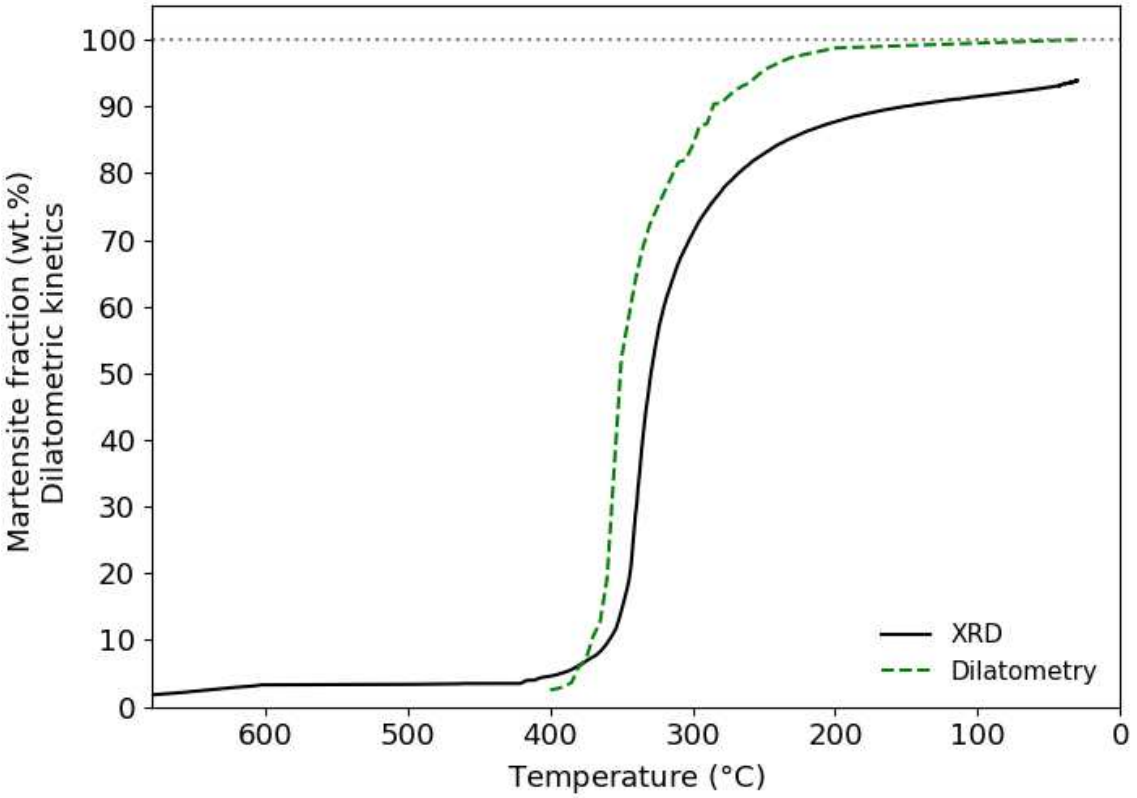

Figure 2: body-centred phase fraction determined by XRD and martensite fraction measured by dilatometry as function of the temperature during the quench. The fractions obtained by dilatometry were calculated from the transformation kinetics and considering the start and end fractions equal to the XRD measurements.

Figure 3(a) shows the relative change in the FWHM of austenite/retained austenite and martensite peaks during the quenching treatment as a function of the temperature. The values have been normalized by the position of the studied peaks. During the cooling between the austenitization temperature down to the Ms temperature, the FWHM of austenite is almost constant as expected, meaning no change in crystallite size and

defect density in the absence of phase transformation and plastic events. The observations are consistent with the literature [12,34]. The cooling rate is too high to enable recovery process. During the first stage of martensite transformation (not following the Koistinen and Marburger's athermal equation), between 394 and 365°C, no notable changes are observed while below 365°C the austenitic FWHMs of all diffraction peaks increase drastically. As the martensite transformation progresses, the austenite FWHMs continue to increase down to the room temperature. For martensite, the observed behavior is rather different. Due to very low peak intensities at the beginning of the transformation, up to 5 wt.% of body-centered phase, the uncertainties are high. The measured FWHMs are thus not relevant down to 365°C. Below this true Ms temperature, a strong increase in the FWHMs is observed. Then the increase slows down when ca. 40 wt.% of martensite is formed, at ca. 350°C.

Different evolutions of the peak broadening with the temperature are experimentally observed for the austenite and for the martensite. A more gradual increase is presented in the former whereas martensite seems to saturate at an early stage of the transformation. While the authors cannot give at the moment a full explanation of the presented different behaviors some elements can be numbered:

- The saturation of the FWHM of the martensite could be partially related to the increase of the martensite fraction, i.e. a newly fraction of martensite with a high FWHM will produce a bigger increase on the average FWHM when the total martensite fraction is low than when martensite fraction is high. A similar reasoning can be postulated for the austenite; as the percentage of the phase decreases the increase of the FWHM in a fraction of the residual phase produces a more important effect on the average FWHM.

- The continuous increase of the FWHM of the austenite might be also a consequence of the martensitic transformation of the austenite with lower dislocation density. Although the high deformed austenite is less stable from a thermodynamic consideration, the crystal defects can mechanically stabilize the mother phase [35]. The transformation of the austenite with a lower dislocation density produces an increase of the average dislocation density observed
- The increase of the peak broadening of the austenite at the final states of the transformation might be also related to the presence of distributions of internal stresses as reported in [36]. The progressive confinement of austenitic regions makes relaxation mechanisms more and more difficult, increasing the residual stresses.

Let us mention that during phase transformation the interpretation of the FWHM is complex since it is affected by several contributions: crystal defects, crystallites size (size of diffraction domains), thermal, chemical and internal stresses heterogeneities within the phases/grains, free surface effects. Due to the set-up used to investigate martensite transformation (transmission mode through the 1,5 mm thickness of the sample), the sample surface effect is low and assumed negligible. In addition investigations showed that the mean crystallites size of both phases are mostly constant. Presently, as the transformation is displacive, no chemical composition distribution is considered (we do not take into account possible self tempering during the martensite transformation). However, there are internal stresses in the phases resulting from the martensitic transformation during cooling due to the phase transformation deformations and their precise knowledge at the different scales is complex and is still an open question. At the scale of the phases, the mean internal stresses generated during

martensitic transformation have been clearly evidenced experimentally by HEXDR [34,37,38]. They are hydrostatic and lead to a shift of the diffraction peaks of the phases.

Internal stress heterogeneities in the martensitic microstructure have been fewly addressed in literature. Thus, on one hand, Archie et al. [39] and Fukui et al. [40] recently reported an anisotropic strain distribution by SEM-FIB based ring-core method at the scale of the martensite variants, while Nakada et al. have reported an anisotropic distribution of the micro residual strains in the austenite [36]. It is possible to assume that the effect of the internal stresses on the FWHM might become more important with the progress of the transformation as the size effect is more important.

In our case, the experimental method used is not able to deconvolute internal stress heterogeneities from the dislocation density contribution within the phases. Nevertheless, the high contribution of the dislocation density to the FWHM in the martensite is supported by the good correlation of the values of dislocation densities measured by TEM and HEXRD in the literature [41] and by our own investigations (TEM: 8×10^{14} 1/m^2, HEXRD: 2×10^{15} 1/m^2).

In our approach we will link the evolutions of FWHM to the evolutions of dislocation densities in both phases.

The Figure 3(b) shows the mean dislocation densities ($\bar{\rho}$), deduced from the FWHMs shown in Figure 3(a) with the modified Williamson-Hall method, in martensite (α) and austenite (γ) as a function of the martensite fraction during the quench. The data have been plotted as a function of the martensite fraction instead of the temperature. As the martensite transformation proceeds, the dislocation density increases both in martensite and in austenite as reported in [12]. This is obviously related to the displacive nature of

the martensitic transformation and the accommodation of the phase transformation strain which affects both the transformation product and the austenitic matrix in which the transformation occurs. (Please note that the densities have been plotted in a log scale).

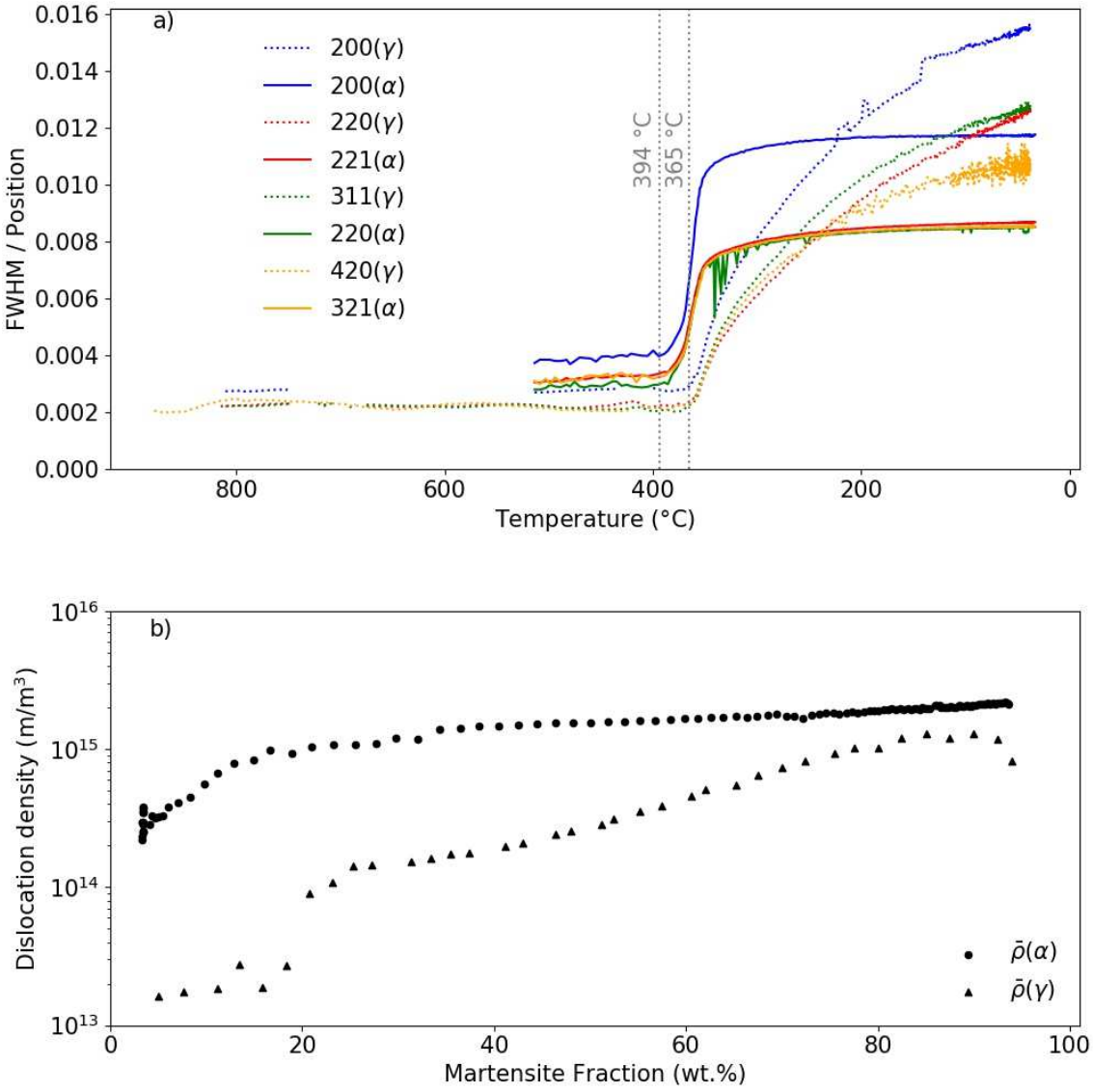

Figure 3: a) FWHMs of austenite (dotted lines) and martensite (continuous lines) diffraction peaks as function of the temperature during the whole studied cooling sequence (after austenitization down to room temperature) and b) deduced mean dislocation densities in both martensite (circle) and austenite (triangles) as a function of the transformed martensite phase fraction.

392 At the beginning of the martensite transformation, preexisting bcc phase shows already
393 a high density of dislocations (2 10^{14} m/m^3). This value lets us suspect that the observed
394 ferritic phase observed prior the martensitic transformation (above 394°C) corresponds
395 in fact to bainitic ferrite appearing just before the martensitic transformation. During the
396 first 20% of the martensitic transformation (mainly occurring below 365°C), the
397 dislocation density increases drastically to reach a value close to 9 10^{14} m/m^3. During
398 the rest of the transformation, down to room temperature, the density of dislocations
399 continues to increase but at an apparent lower rate, to reach a final value of 2 10^{15} m/m^3.
400 This value is in good agreement with the values generally reported at RT in low carbon
401 martensitic steels [42,43]. By TEM observations in a Fe-0.18C steel, Morito et al.
402 reported for instance mean densities around 1.1 10^{15} m/m^3 [41]. The mean dislocation
403 density in martensite phase is thus 10 times higher at the end of the transformation
404 compared to the very first 5 wt.% transformed. It should be emphasized that the
405 dispersion of values along the transformation is lower than in the study of Christien et
406 al. [12]. This has been permitted by our faster acquisition rate (10 Hz). At the fastest
407 transformation rates (around 350°C), diffractograms and thus dislocation densities are
408 measured every 2.5% of transformed martensite. The evolution of the dislocation
409 density of the martensite does not present a linear tendency as reported by Christien et
410 al. [12], thus, a square root function was chosen to fit the experimental data by its
411 simplicity and general acceptable fit as can be observed in Figure 4.
412 The evolution of the dislocation density in the austenite does not saturate before 80
413 wt.% of martensite is formed. The evolutions in austenite and in martensite seem
414 correlated. Before the martensitic transformation, the density is 1.7 10^{13} m/m^3 as
415 expected from an austenitic phase annealed at high temperature. The density increases

during the first 15% of transformation to reach 8 10^{13} m/m^3. After this apparent first fast regime, the density continues to increase very rapidly but at almost the same rate. It should be noted that the data scattering is higher in austenite than in martensite at the beginning of the transformation. This is related to the low density values reported in that case. However, the measured values do not evolve much during the cooling before the martensitic transformation, as shown in Figure 3(a). This permits to ascertain the determination procedure described above, as no plastic events are expected in austenite.

Discussion

The discussion will be segmented in three parts. The first will focus on the insight brought by the dislocation density measurements in the martensite phase during cooling. The succeeding section will analyze the effect of the dislocation density on the austenite strength and the last one is dedicated to analyze the distribution of local and spatial yield strength distribution in martensite due to the distribution of dislocation densities.

Instantaneous dislocation density in martensite:

The studied steel shows at room temperature a very conventional lath martensitic microstructure as observed by [9] on similar steels. It is now well admitted that this typical microstructure appears in a displacive way by the nucleation of new laths; gathered into blocks of similar variants and packets of coplanar variants inside prior austenite grains [9]. As said in the introduction, the size, the dislocation structure, the

segregations, the residual stresses and thus the local strength of these laths at room temperature should strongly depend on their respective transformation temperatures.

As a consequence, it is likely that the dislocations are not homogeneously distributed in the final martensitic microstructure.

The increase in the mean dislocation density in martensite during the transformation can be interpreted either by the fact that already formed laths undergo plastic deformation or by the fact that new laths present a higher dislocations density than the previous ones arising the mean value. The plastic deformation in already formed lath structures is unlikely for at least two reasons. First of all, plastic accommodations due to the transformation strain will occur to a large extent in the softest phase, i.e. here in the austenite. This is the reason why its mean dislocation density increases drastically all along the transformation contrary to martensite. Secondly, higher degree of plastic interactions is expected after the percolation of the martensitic structure (about typically 20%-30% of transformation) [37,44]. Figure 3(b) shows on the contrary, a decrease in the rate of dislocation creation. As a consequence, we assume that the increase in the mean dislocation density in martensite is due the progressive nucleation of new laths containing more dislocations than the previous ones. Since the data are acquired all along the martensite phase transformation, it is possible to determine the dislocation density in these new laths, considering that the forming martensite lath is not affected by the earlier ones. It is also assumed that recovery process that could occur during martensite tempering is surely limited due to the applied cooling rate. However possible self-tempering (carbon segregation, carbide precipitation) cannot be ruled out even if no carbide can be observed and identified on the diffractograms.

In the following, we call the instantaneous dislocation density $\rho^{inst.}$ the dislocation density in the laths forming when the martensite fraction is F. At the beginning of the transformation, the instantaneous density is equal to the mean density of course. With what is said before, this function progressively increases and contributes to increase the mean density of dislocations ($\overline{\rho}$) in previously formed martensite F. By construction, it comes:

$$\overline{\rho} = 1/F \int_0^F \rho^{inst}(f)\, df \qquad (2)$$

By deriving Equation (2) with respect to F, the instantaneous density of dislocations at F is given by:

$$d(F\,\overline{\rho}(F)) = \rho^{inst}(F)dF \qquad (3)$$

Using a step by step integration, the instantaneous dislocation density for martensite is plotted in Figure 4.

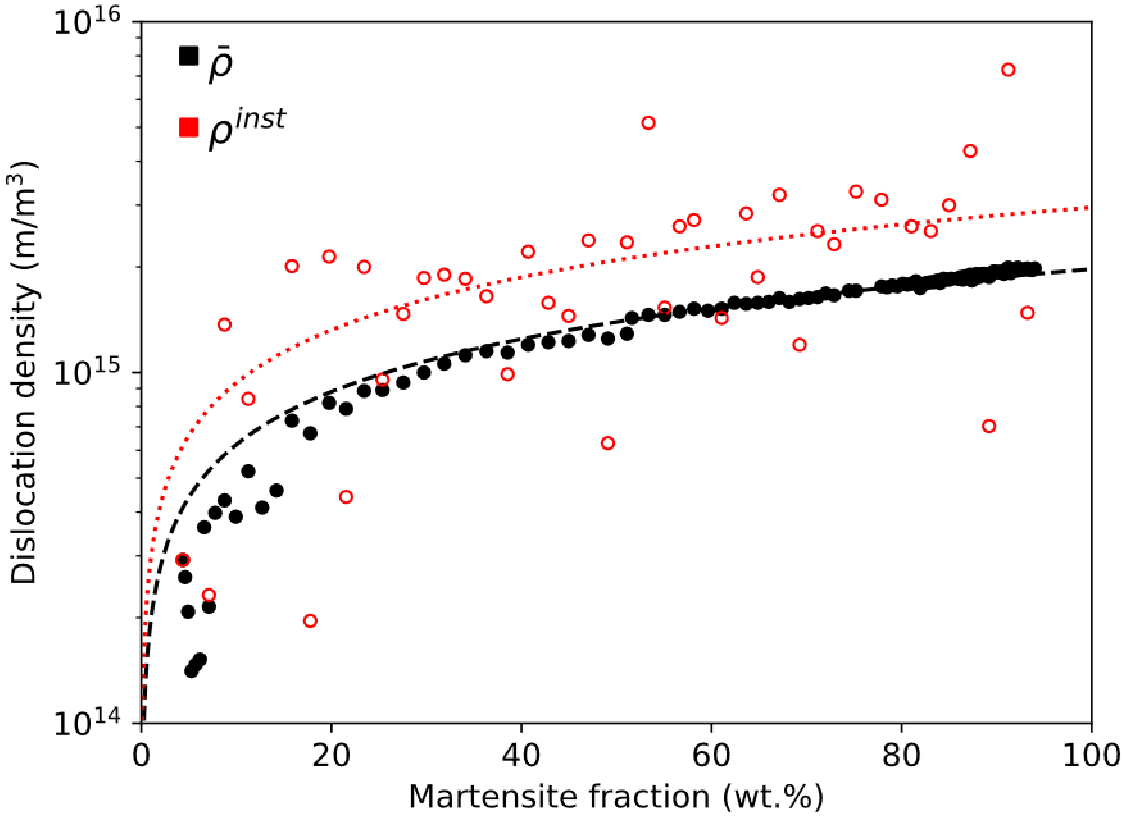

480

481 *Figure 4: Mean dislocation density (filled circles) and instantaneous dislocation density*
482 *calculated with ca. 2 wt.% steps (hollow circles) in martensite as a function of the martensite*
483 *phase fraction during the quenching. The black discontinuous line corresponds to an empirical*
484 *square-root law calibrated on the experimental results for a better readability of the results,*
485 *while the red dotted continuous line corresponds to the analytical solution related to the*
486 *empirical square-root law calibrated.*

487

488 As the transformation moves forward, the new formed martensite laths contain a higher
489 dislocation density than the earlier ones. This increase can be explained by the fact that
490 the first martensite fraction is formed in a soft austenitic matrix. The following
491 martensite laths would form in a harder matrix and with higher shearing modulus
492 (temperature decrease) [12,27]. The inheritance of the austenite dislocation structure
493 into martensite may also contribute to the total dislocation density in martensite. In fact,
494 the final dislocation density in austenite at room temperature represents about 30% of
495 the dislocation density expected in the very last formed laths of martensite.

Dislocations and strength of austenite

The dislocation density in the austenite before the martensitic transformation is of the order of 10^{13} m/m^3 and increases with a rate higher than in the martensite during the transformation. For the austenite phase, ρ^{inst} is not presented as the increase in the mean dislocation density cannot reasonably be explained by a martensite transformation occurring solely in the dislocation poor austenitic grains. The increase results more probably from a progressive plasticization due to the accommodation of the transformation strains. However, it is likely that dislocations are not well and homogeneously distributed. This could explain in some extent the dispersions observed in the values at the beginning of the transformation.

The final dislocation density in austenite is 1 10^{15} m/m^3 at room temperature. This density is even higher than the ones found in the very first laths of martensite. Dislocations contribute to hardening, and this contribution σ_{disl}, can be calculated with the Taylor equation [45]:

$$\sigma_{disl} = \alpha C_T \mu b \rho^{-½} \qquad (4)$$

where α is a geometrical constant equal to 0.4, C_T the Taylor factor equal to 3, μ is the shearing modulus (84 GPa), b and ρ are respectively the Burgers vectors (2.5 10^{-10}m) of perfect dislocations in martensite and the mean dislocation density in austenite. The shear modulus was calculated at room temperature taking into account the steel composition [46].

The contribution to hardening of dislocations due to the martensitic transformation is thus equal to ca. 795 MPa in austenite. Retained austenite in martensite is thus far from being a soft phase, especially since the previous contribution does not account for solid

521 solution hardening and size effect. In fact, retained austenite is often located as thin
522 films in between martensite laths.
523 As a consequence, austenite cannot contribute to the plastic behavior of martensitic
524 microstructures, at least not as much as supposed by certain models [47]. Retained
525 austenite is in fact already intensively plasticized at room temperature due to the
526 transformation strain and thus is also a hard phase of the microstructure.
527
528 Local and spatial yield strength distribution in martensite:
529 The instantaneous dislocation density shown in Figure 4 introduced a dislocation
530 density distribution inside the martensite laths. The first formed at high temperatures
531 (lower martensite fraction) show a lower dislocation density than those formed at lower
532 temperature (higher martensite fraction). As a consequence, the contribution of
533 dislocations to their respective hardening are surely different. Applying again the Taylor
534 equation to the instantaneous density of dislocations instead of the average dislocation
535 density permits to estimate the related distribution of strengths in the microstructure.
536 The parameters used are α=0.4, C_T=3, b=2.5 10^{-10}m, and μ the shearing modulus for a
537 martensite with the initial steel composition (76 GPa). The method presented in the
538 present work allows to estimate the dislocation hardening contribution to the yield
539 strength in the forming martensite during the whole cooling, as shown in the Figure 5.
540 Figure 5(a) shows the dislocation contribution to the yield strength of the instantaneous
541 dislocation density, for increasing F values. The Taylor equation was applied
542 considering each instantaneous dislocation density while the newly formed phase
543 fraction was summed to the total transformed martensite, allowing to show the increase

544 of the dislocation strengthening with the martensite transformation. As expected, a
545 similar trend with the instantaneous dislocation density in martensite phase is observed.

546 The dislocation contribution to the yield strength is two times higher in the last formed
547 martensite lath than in the first one, respectively ca. 1250 and 500 MPa.

548 The density of probability of yielding at a given stress caused by the dislocations
549 density distribution (called stress spectrum f(σ)) was obtained by evaluating the
550 dislocation hardening related to each newly formed martensite between the limits of 50
551 MPa bins from 0 to 4500 MPa. Once the bin in which the dislocation hardening
552 belonged was identified (evaluated with the empirical root-law calculated instantaneous
553 dislocation density, red dotted curve in Figure 4), the newly formed martensite fraction
554 was summed to the fraction related to that interval.

555 By this method, at the end of the transformation, it was possible to obtain the total
556 martensite fraction for each bin of 50 MPa. The following step was to normalize the
557 integral of the fractions versus the local yield strength in order to obtain a distribution of
558 probability which integral would be equal to 1 (the whole martensite transformed).

559 The mentioned density of probability has been plotted and presented Figure 5(b). The
560 first spike in the obtained distribution is due to the fact that in the first calculated point
561 the amount of fraction already transformed is significant.

562 The obtained distribution has been compared to the stress spectrum calculated by the
563 Continuous Composite Approach (CCA) [2] to explain the behavior of the studied
564 steels. The stress spectrum, $f(\sigma)$, in the CCA is obtained by reverse resolution of the
565 following equation:
566

$$\Sigma = \int_{\sigma min}^{\sigma L} f(\sigma)\,\sigma\,d\sigma + \sigma_L \int_{\sigma L}^{+\infty} f(\sigma)\,d\sigma \qquad (5)$$

where Σ is the macroscopic stress, σ_{min} is the minimum value in the local yield stress spectrum, σ_L is the stress state of phases remaining elastic.

The CCA distribution presented in this work is obtained by the calculated tensile behavior of the studied alloy (0.215wt.% C) with [2]. In the CCA, all the contributions affect the distribution as solid solution strengthening due to carbon and substitutional alloying elements, friction of pure iron, internal stresses, dislocation densities. It explains the initial shift at higher strength of the distribution expected from the CCA compared to the distribution obtained by the dislocation density distribution alone. It also clearly appears that the ratio between the harder and the softer fraction formed (ca. 2.5 considering the dislocation distribution only) is lower than the actual ratio expected by the CCA model (ca. 6). The higher values of the density of probability of spectrum due to the dislocation hardening are due to that both curves are normalized and the lower ratio of this spectrum.

The lower ratio of the spectrum due to the dislocation density distribution means that the measured distributions of dislocations in martensite is not sufficient alone to explain the micromechanical behavior of the steel. Dislocation strengthening is not the sole contribution of the local yield of martensitic laths. As shown by Morsdorf et al. [9], the lath size effect must evidently be considered, but according to Badinier [10], the obtained spread of local yield is far from being sufficient to explain the stress spectrum. Different degrees of self-tempering (carbide precipitation and carbon segregations) are also expected in martensite [48] but they cannot explain the behavior of martensite by themselves as shown by Hutchinson et al. [4].

591 Hutchinson et al. introduces calculated residual stress heterogeneities in the martensite
592 (at the scale of the grains) resulting from the phase transformation during cooling to
593 predict the tensile behavior of martensite microstructure [4]. The main assumption of
594 the authors was to consider that the stress gradient contribution on the martensite
595 FWHM is alone able to describe the martensite FWHM decrease during the tensile test
596 as observed experimentally. However, it is well known that other contributions are
597 present as tetragonality even for low carbon steels [49], crystallite size, dislocation
598 density.
599 We consider that the distribution of flow stress (which could describe the stress-strain
600 curve) in the martensite is originated by the microstructure principally (laths sizes,
601 dislocations densities); internal stresses contribute to the phenomenon without being the
602 only explanation as reported by Wang et al. [50]. Indeed, if the FWHMs are only due to
603 the internal stresses and decrease with the further deformation (as reported by
604 Hutchinson et al. [4]), the Bauschinger effect would decrease as well which is the
605 opposite to the experimental observation [2,10,50].
606 Hence, it appears from this work that the local yield strength distribution in martensite
607 is the result of a complex convolution of different mechanisms, having their own spatial
608 distributions. However, it seems that the distribution of dislocation densities is one of
609 the most important sources of spread (nearly one half of the distribution width),
610 contrary to lath size distribution.
611 The functional form for the local yield stress spectrum in the CCA model (an Avrami
612 type law [2]) can be selected differently based on the type of distribution found
613 experimentally. However, for obtaining the real local yield stress spectrum not only the
614 distribution of dislocation densities has to be considered, but also the other previously

615 mentioned spatial distributions. The convolution of the mentioned distributions might
616 produce a different type of functional form than the one that might be inferred only
617 from the distribution of the dislocation densities. As consequence, the authors do not
618 find convenient at the moment change the functional form, while the mentioned
619 modification might be address subsequently while analyzing the other sources of
620 distributions.

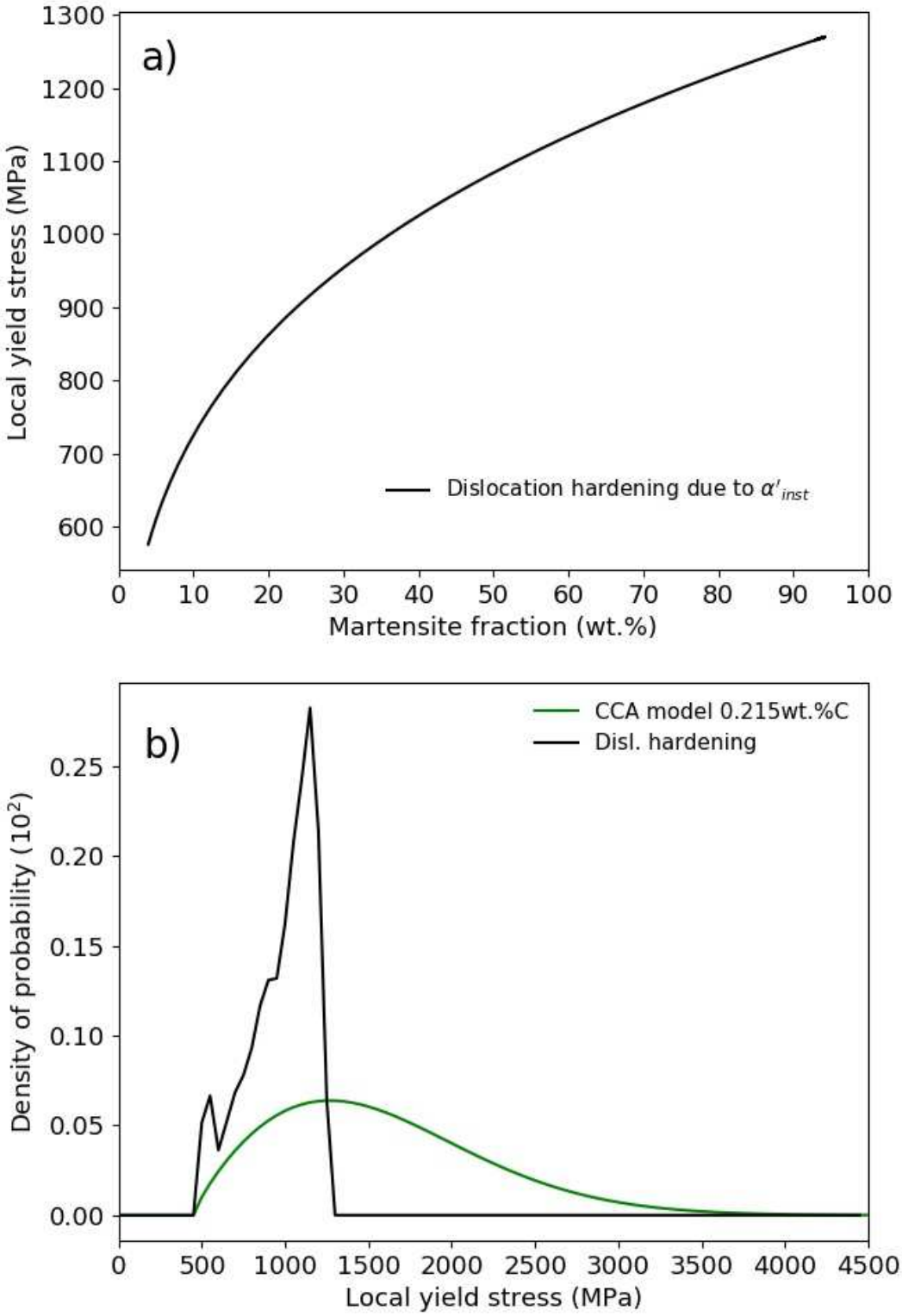

621

622 *Figure 5: a) The dislocation contribution to the yield stress for each newly formed martensite*
623 *fraction b) The density probability to find a lath with a given local yield stress considering only*

the measured dislocation. These experimental values are compared to the expected stress distribution necessary to explain the mechanical behavior of the studied steel according to [2].

Conclusion

The evolution of the dislocation densities in martensite and in austenite during the quench of a low-carbon (0.215wt.%C) steel has been investigated in situ by the mean of X-ray diffraction experiments on a synchrotron beamline. These measurements were conducted with the mWH methodology developed by Ungar et al. and a more conventional Rietveld refinement. The line configuration offers an excellent time resolution adapted to the kinetics of the studied steels.

The mean dislocations density in martensite was shown to increase progressively as the martensitic transformation proceeds confirming that dislocations are not homogeneously distributed between the laths, in agreement with recent post mortem observations. The resulting spatial distribution has been estimated introducing the concept of instantaneous dislocation density in martensite. The associated spread in the local yield strengths of laths has been compared to the one calculated on a micromechanical basis (CCA approach), i.e. based on an inverse analysis from the macroscopic mechanical behavior. It was shown that microstructural heterogeneities (dislocation densities, lath sizes, carbon segregations) as well as internal stresses resulting from the transformation deformation must be taken into account to explain the unique behavior of these steels [50]. The density of dislocations appears to be a major contribution explaining almost one half of the stress distribution.

The evolution of the dislocation density in austenite has also been analyzed in details and discussed at the light of the martensite transformation strains. Low carbon

martensitic steels contain significant fraction of retained austenite but this latter phase cannot be considered as a soft phase as it contains almost the same density of dislocations as the martensite. The strength of retained austenite is necessarily higher than the softest martensite lath as it contains 10 times higher density of dislocations. Hence, retained austenite cannot be considered as the interphase medium permitting to explain the plastic deformation of martensitic microstructures (if excluding TRIP effect).

Acknowledgements

This work was funded by the i-SITE Lorraine Université d'Excellence program (LUE) and supported by ArcelorMittal Maizières les Metz (Product Research Centre). The HEXRD experiments were conducted at DESY (PETRAIII-P07 beamline) in Hamburg under the I-20180973 EC grant. A special thanks is dedicated to the team of the P-07 line. The expertise of N. Schell and A. Stark was much appreciated and widely contributed to the success of the study.

The Laboratory of Excellence on Design of Alloy Metals for low-mAss Structures (Labex DAMAS) from the Université de Lorraine (France) is also fully acknowledged for its support.

Conflicts of Interest

The authors declare no conflict of interest. The funders had no role in the design of the study; in the collection, analyses, or interpretation of data; in the writing of the manuscript, or in the decision to publish the results.

Data availability

The raw/processed data required to reproduce these findings cannot be shared at this time as the data also forms part of an ongoing study.

References

[1] N. Fonstein, ADVANCED HIGH STRENGTH SHEET STEELS : physical metallurgy, design, processing, and properties., SPRINGER, 2016.

[2] S. Allain, O. Bouaziz, M. Takahashi, Toward a New Interpretation of the Mechanical Behaviour of As-quenched Low Alloyed Martensitic Steels, ISIJ Int. 52 (2012) 717–722. https://doi.org/10.2355/isijinternational.52.717.

[3] T. Ungár, S. Harjo, T. Kawasaki, Y. Tomota, G. Ribárik, Z. Shi, Composite Behavior of Lath Martensite Steels Induced by Plastic Strain, a New Paradigm for the Elastic-Plastic Response of Martensitic Steels, Metall. Mater. Trans. A Phys. Metall. Mater. Sci. 48 (2017) 159–167. https://doi.org/10.1007/s11661-016-3845-4.

[4] B. Hutchinson, P. Bate, D. Lindell, A. Malik, M. Barnett, P. Lynch, Plastic yielding in lath martensites – An alternative viewpoint, Acta Mater. 152 (2018) 239–247. https://doi.org/10.1016/j.actamat.2018.04.039.

[5] J. Li, T. Ohmura, K. Tsuzaki, Microstructure effect on nanohardness distribution

692 for medium-carbon martensitic steel, Sci. China, Ser. E Technol. Sci. 49 (2006)
693 10–19. https://doi.org/10.1007/s11431-004-5228-0.
694 [6] B.B. He, M.X. Huang, Revealing the Intrinsic Nanohardness of Lath Martensite
695 in Low Carbon Steel, Metall. Mater. Trans. A Phys. Metall. Mater. Sci. 46 (2015)
696 688–694. https://doi.org/10.1007/s11661-014-2681-7.
697 [7] B.B. He, K. Zhu, & M.X. Huang, On the nanoindentation behaviour of complex
698 ferritic phases, Philos. Mag. Lett. (2014).
699 https://doi.org/10.1080/09500839.2014.921348.
700 [8] L. Morsdorf, O. Jeannin, D. Barbier, M. Mitsuhara, D. Raabe, C.C. Tasan,
701 Multiple mechanisms of lath martensite plasticity, Acta Mater. 121 (2016) 202–
702 214. https://doi.org/10.1016/j.actamat.2016.09.006.
703 [9] L. Morsdorf, C.C. Tasan, D. Ponge, D. Raabe, 3D structural and atomic-scale
704 analysis of lath martensite: Effect of the transformation sequence, Acta Mater. 95
705 (2015) 366–377. https://doi.org/10.1016/j.actamat.2015.05.023.
706 [10] G. Badinier, Effect of Carbon Segregation and Carbide Precipitation on the
707 Mechanical Response of Martensite, University of British Columbia, 2013.
708 https://doi.org/10.14288/1.0073612.
709 [11] G. Badinier, C.W. Sinclair, X. Sauvage, X. Wang, V. Bylik, M. Gouné, F. Danoix,
710 Microstructural heterogeneity and its relationship to the strength of martensite,
711 Mater. Sci. Eng. A. 638 (2015) 329–339.
712 https://doi.org/10.1016/j.msea.2015.04.088.
713 [12] F. Christien, M.T.F. Telling, K.S. Knight, Neutron diffraction in situ monitoring
714 of the dislocation density during martensitic transformation in a stainless steel,
715 Scr. Mater. 68 (2013) 506–509. https://doi.org/10.1016/j.scriptamat.2012.11.031.

[13] G. Ashiotis, A. Deschildre, Z. Nawaz, J.P. Wright, D. Karkoulis, F.E. Picca, J. Kieffer, The fast azimuthal integration Python library: PyFAI, J. Appl. Crystallogr. 48 (2015) 510–519. https://doi.org/10.1107/S1600576715004306.

[14] S. Allain, S. Aoued, A. Quintin-Poulon, M. Gouné, F. Danoix, J.-C. Hell, M. Bouzat, M. Soler, G. Geandier, In Situ Investigation of the Iron Carbide Precipitation Process in a Fe-C-Mn-Si Q&P Steel, Materials (Basel). 11 (2018) 1087. https://doi.org/10.3390/ma11071087.

[15] G.K. Williamson, W.H. Hall, X-ray line broadening from filed aluminium and wolfram, Acta Metall. 1 (1953) 22–31. https://doi.org/10.1016/0001-6160(53)90006-6.

[16] N. Sallez, X. Boulnat, A. Borbély, J.L. Béchade, D. Fabrègue, M. Perez, Y. De Carlan, L. Hennet, C. Mocuta, D. Thiaudière, Y. Bréchet, In situ characterization of microstructural instabilities: Recovery, recrystallization and abnormal growth in nanoreinforced steel powder, Acta Mater. 87 (2015) 377–389. https://doi.org/10.1016/j.actamat.2014.11.051.

[17] P.S.-Iuc.M. on Crystallography, undefined 1993, The Rietveld Method, edited by RA Young, (n.d.).

[18] T. Ungár, A. Borbély, The effect of dislocation contrast on x-ray line broadening: A new approach to line profile analysis, Appl. Phys. Lett. 69 (1996) 3173–3175. https://doi.org/10.1063/1.117951.

[19] N. Sallez, X. Boulnat, A. Borbély, J.L. Béchade, D. Fabrègue, M. Perez, Y. De Carlan, L. Hennet, C. Mocuta, D. Thiaudière, Y. Bréchet, In situ characterization of microstructural instabilities: Recovery, recrystallization and abnormal growth in nanoreinforced steel powder, Acta Mater. 87 (2015) 377–389.

https://doi.org/10.1016/j.actamat.2014.11.051.

[20] T. Ungár, I. Dragomir, Á. Révész, A. Borbély, The contrast factors of dislocations in cubic crystals: the dislocation model of strain anisotropy in practice, J. Appl. Crystallogr. 32 (1999) 992–1002. https://doi.org/10.1107/s0021889899009334.

[21] T. Ungár, G. Tichy, The Effect of Dislocation Contrast on X-Ray Line Profiles in Untextured Polycrystals, Phys. Status Solidi. 171 (1999) 425–434. https://doi.org/10.1002/(SICI)1521-396X(199902)171:2<425::AID-PSSA425>3.0.CO;2-W.

[22] S. Takaki, T. Masumura, T. Tsuchiyama, Proposal of simplified modified Williamson-Hall equation, ISIJ Int. 58 (2018) 2354–2356. https://doi.org/10.2355/isijinternational.ISIJINT-2018-517.

[23] Z.M. Shi, W. Gong, Y. Tomota, S. Harjo, J. Li, B. Chi, J. Pu, Study of tempering behavior of lath martensite using in situ neutron diffraction, Mater. Charact. 107 (2015) 29–32. https://doi.org/10.1016/j.matchar.2015.06.040.

[24] A. Borbély, J. Dragomir-Cernatescu, G. Ribárik, T. Ungár, Computer program *ANIZC* for the calculation of diffraction contrast factors of dislocations in elastically anisotropic cubic, hexagonal and trigonal crystals, J. Appl. Crystallogr. 36 (2003) 160–162. https://doi.org/10.1107/S0021889802021581.

[25] J. Leese, A.E. Lord, Elastic stiffness coefficients of single-crystal iron from room temperature to 500°C, J. Appl. Phys. 39 (1968) 3986–3988. https://doi.org/10.1063/1.1656884.

[26] D.J. Dever, Temperature dependence of the elastic constants in α-iron single crystals: Relationship to spin order and diffusion anomalies, J. Appl. Phys. 43 (1972) 3293–3301. https://doi.org/10.1063/1.1661710.

764 [27] D.G. Isaak, K. Masuda, Elastic and viscoelastic properties of α iron at high
765 temperatures, J. Geophys. Res. 100 (1995). https://doi.org/10.1029/95jb01235.
766 [28] Y. Zhao, L. Le Joncour, A. Baczmański, E. Gadalińska, S. Wroński, B. Panicaud,
767 M. François, C. Braham, T. Buslaps, Stress distribution correlated with damage in
768 duplex stainless steel studied by synchrotron diffraction during plastic necking,
769 Mater. Des. 113 (2016) 157–168. https://doi.org/10.1016/j.matdes.2016.10.014ï.
770 [29] H.S. Yang, H.K.D.H. Bhadeshia, Uncertainties in dilatometric determination of
771 martensite start temperature, Mater. Sci. Technol. 23 (2007) 556–560.
772 https://doi.org/10.1179/174328407X176857.
773 [30] S.M.C. van Bohemen, J. Sietsma, The kinetics of bainite and martensite
774 formation in steels during cooling, Mater. Sci. Eng. A. 527 (2010) 6672–6676.
775 https://doi.org/10.1016/j.msea.2010.06.091.
776 [31] S.M.C. van Bohemen, L. Morsdorf, Predicting the Ms temperature of steels with
777 a thermodynamic based model including the effect of the prior austenite grain
778 size, Acta Mater. 125 (2017) 401–415.
779 https://doi.org/10.1016/j.actamat.2016.12.029.
780 [32] S.M.C. van Bohemen, Bainite and martensite start temperature calculated with
781 exponential carbon dependence, Mater. Sci. Technol. 28 (2012) 487–495.
782 https://doi.org/10.1179/1743284711Y.0000000097.
783 [33] H.K.D.H. Bhadeshia, Thermodynamic extrapolation and martensite-start
784 temperature of substitutionally alloyed steels, Met. Sci. 15 (1981) 178–180.
785 https://doi.org/10.1179/030634581790426697.
786 [34] Y. Wang, Y. Tomota, T. Ohmura, S. Morooka, W. Gong, S. Harjo, Real time
787 observation of martensite transformation for a 0.4C low alloyed steel by neutron

788 diffraction, Acta Mater. 184 (2020) 30–40.
789 https://doi.org/10.1016/j.actamat.2019.11.051.
790 [35] A.A.P. K. SIPOS, L. REMY, A, Q.P. Analysis, Influence of Austenite
791 Predeformation on Mechanical Properties and Strain-Induced Martensitic
792 Transformations of a High Manganese Steel, Metall. Trans. A. 7 (1976).
793 [36] N. Nakada, Y. Ishibashi, T. Tsuchiyama, S. Takaki, Self-stabilization of
794 untransformed austenite by hydrostatic pressure via martensitic transformation,
795 Acta Mater. 110 (2016) 95–102. https://doi.org/10.1016/j.actamat.2016.03.048.
796 [37] S.Y.P. Allain, S. Gaudez, G. Geandier, J.C. Hell, M. Gouné, F. Danoix, M. Soler,
797 S. Aoued, A. Poulon-Quintin, Internal stresses and carbon enrichment in austenite
798 of Quenching and Partitioning steels from high energy X-ray diffraction
799 experiments, Mater. Sci. Eng. A. 710 (2018) 245–250.
800 https://doi.org/10.1016/j.msea.2017.10.105.
801 [38] M. Dehmas, F. Bruneseaux, G. Geandier, E. Gautier, B. Appolaire, S. Denis, B.
802 Denand, A. Settefrati, A. Mauro, M. Peel, G. Gonzales Aviles, T. Buslaps, Apport
803 de la diffraction synchrotron à l'étude de la transformation martensitique dans les
804 aciers, Matériaux Tech. 97 (2009) 61–69.
805 https://doi.org/10.1051/mattech/2010012.
806 [39] F. Archie, M.Z. Mughal, M. Sebastiani, E. Bemporad, S. Zaefferer, Anisotropic
807 distribution of the micro residual stresses in lath martensite revealed by FIB ring-
808 core milling technique, Acta Mater. 150 (2018) 327–338.
809 https://doi.org/10.1016/j.actamat.2018.03.030.
810 [40] D. Fukui, N. Nakada, S. Onaka, Internal residual stress originated from Bain
811 strain and its effect on hardness in Fe–Ni martensite, Acta Mater. 196 (2020)

660–668. https://doi.org/10.1016/j.actamat.2020.07.013.

[41] S. Morito, J. Nishikawa, T. Maki, Dislocation Density within Lath Martensite in Fe–C and Fe–Ni Alloys, ISIJ Int. 43 (2003) 1475–1477. https://doi.org/10.2355/isijinternational.43.1475.

[42] G. Krauss, Martensite in steel: strength and structure, Mater. Sci. Eng. A. 273–275 (1999) 40–57. https://doi.org/10.1016/S0921-5093(99)00288-9.

[43] D.C. Saha, E. Biro, A.P. Gerlich, Y. Zhou, Effects of tempering mode on the structural changes of martensite, Mater. Sci. Eng. A. 673 (2016) 467–475. https://doi.org/10.1016/j.msea.2016.07.092.

[44] S. Nambu, N. Shibuta, M. Ojima, J. Inoue, T. Koseki, H.K.D.H. Bhadeshia, In situ observations and crystallographic analysis of martensitic transformation in steel, Acta Mater. 61 (2013) 4831–4839. https://doi.org/10.1016/j.actamat.2013.04.065.

[45] G.I. Taylor, Plastic Strain in Metals, J. Inst. Met. 62 (1938) 307-.

[46] G. Ghosh, G.B. Olson, The isotropic shear modulus of multicomponent Fe-base solid solutions, Acta Mater. 50 (2002) 2655–2675. https://doi.org/10.1016/S1359-6454(02)00096-4.

[47] F. Maresca, V.G. Kouznetsova, M.G.D. Geers, Deformation behaviour of lath martensite in multi-phase steels, Scr. Mater. 110 (2016) 74–77. https://doi.org/10.1016/j.scriptamat.2015.08.004.

[48] B. Hutchinson, J. Hagström, O. Karlsson, D. Lindell, M. Tornberg, F. Lindberg, M. Thuvander, Microstructures and hardness of as-quenched martensites (0.1-0.5%C), Acta Mater. 59 (2011) 5845–5858. https://doi.org/10.1016/j.actamat.2011.05.061.

[49] N. Maruyama, S. Tabata, H. Kawata, Excess Solute Carbon and Tetragonality in As-Quenched Fe-1Mn-C (C:0.07 to 0.8 Mass Pct) Martensite, Metall. Mater. Trans. A Phys. Metall. Mater. Sci. 51 (2020) 1085–1097. https://doi.org/10.1007/s11661-019-05617-y.

[50] L.Y. Wang, Y.X. Wu, W.W. Sun, Y. Bréchet, L. Brassart, A. Arlazarov, C.R. Hutchinson, Strain hardening behaviour of as-quenched and tempered martensite, Acta Mater. (2020). https://doi.org/10.1016/j.actamat.2020.08.067.

844 Experience 1

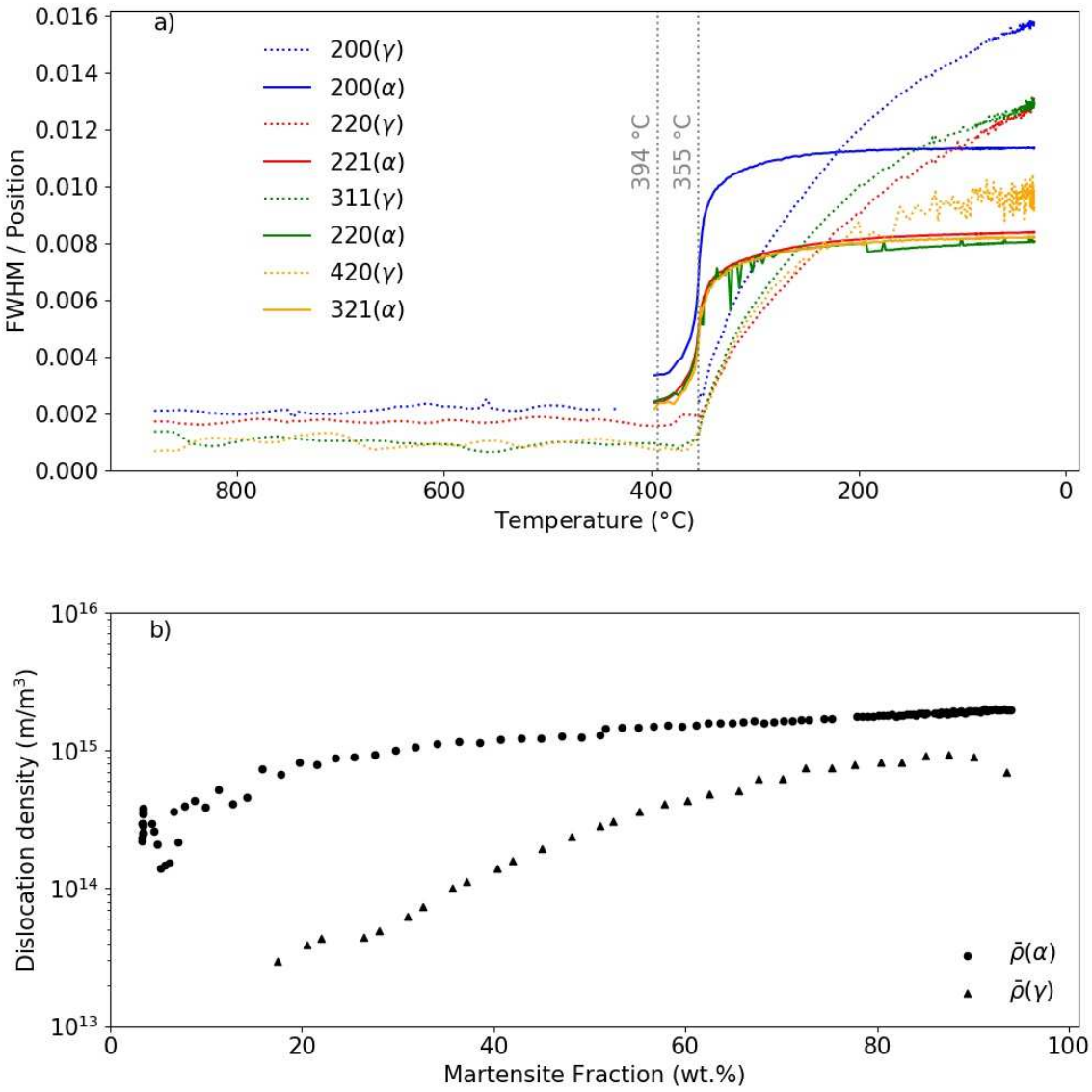

845

846 *Figure 6: a) FWHMs of austenite (dotted lines) and martensite (continuous lines) diffraction*
847 *peaks as function of the temperature during the whole studied cooling sequence (after*
848 *austenitization down to room temperature) and b) deduced mean dislocation densities in both*
849 *martensite (circle) and austenite (triangles) as a function of the transformed martensite phase*
850 *fraction.*

851

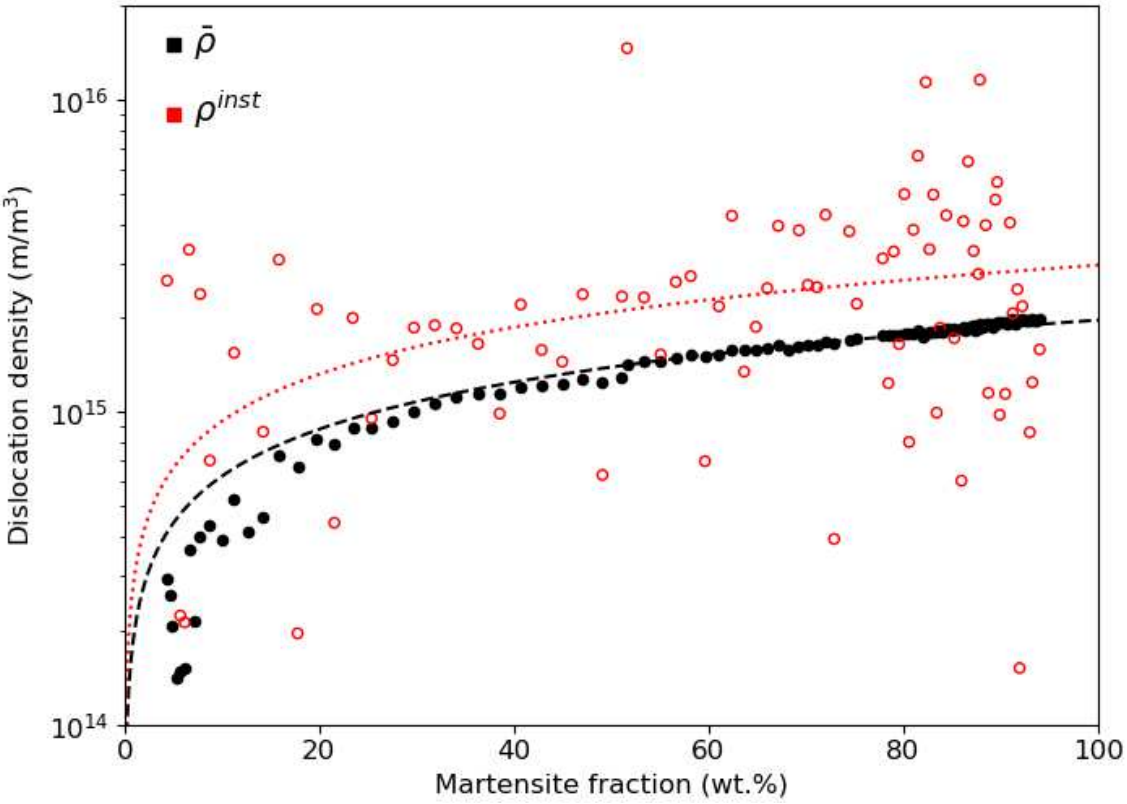

Figure 7: Mean dislocation density (filled circles) and instantaneous dislocation density (hollow circles) in martensite as a function of the martensite phase fraction during the quenching. The black discontinuous line corresponds to an empirical square-root law calibrated on the experimental results for a better readability of the results, while the red dotted continuous line corresponds to the analytical solution related to the empirical square-root law calibrated.

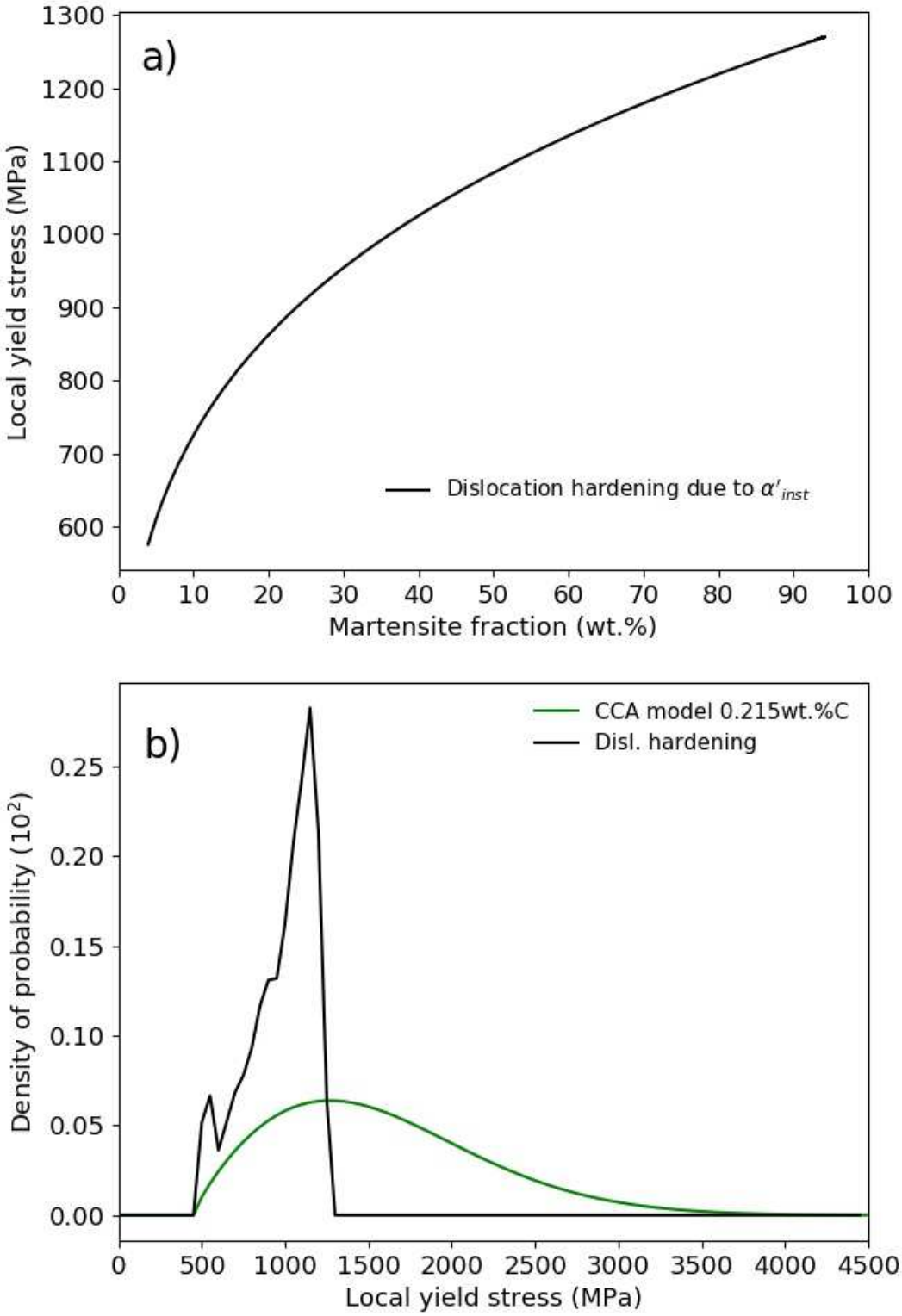

858

859 *Figure 8: a) The dislocation contribution to the yield stress for each newly formed martensite*
860 *fraction b) The density probability to find a lath with a given local yield stress considering only*
861 *the measured dislocation. These experimental values are compared to the expected stress*
862 *distribution necessary to explain the mechanical behavior of the studied steel according to* [2].

Experience 2

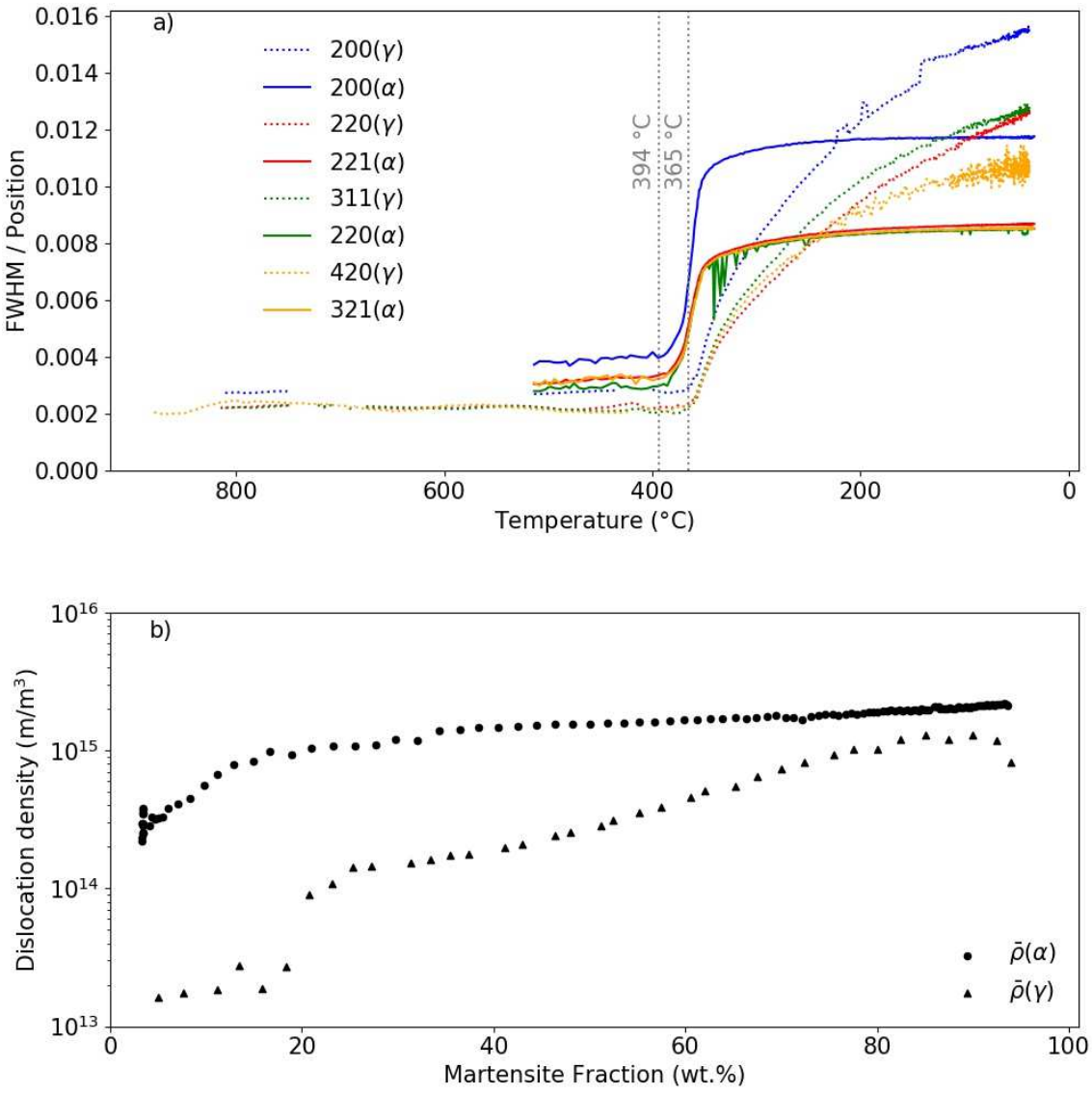

Figure 9: a) FWHMs of austenite (dotted lines) and martensite (continuous lines) diffraction peaks as function of the temperature during the whole studied cooling sequence (after austenitization down to room temperature) and b) deduced mean dislocation densities in both martensite (circle) and austenite (triangles) as a function of the transformed martensite phase fraction.

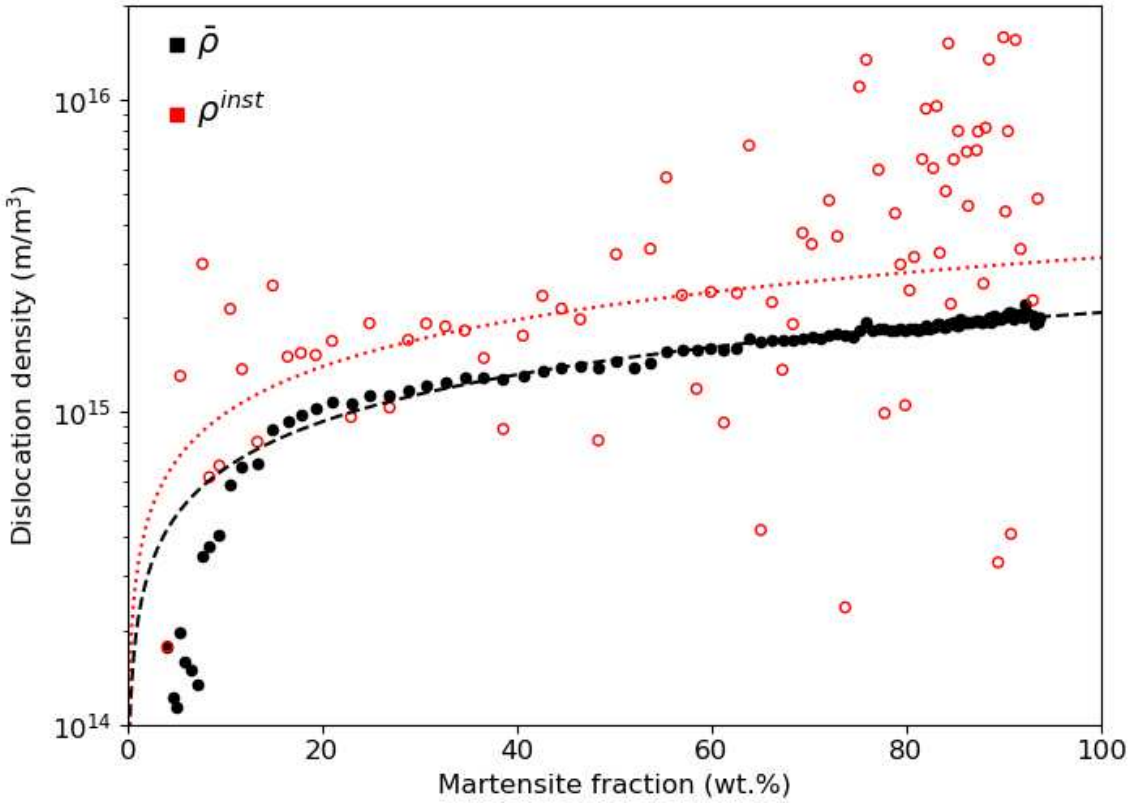

Figure 10: Mean dislocation density (filled circles) and instantaneous dislocation density (hollow circles) in martensite as a function of the martensite phase fraction during the quenching. The black discontinuous line corresponds to an empirical square-root law calibrated on the experimental results for a better readability of the results, while the red dotted continuous line corresponds to the analytical solution related to the empirical square-root law calibrated.

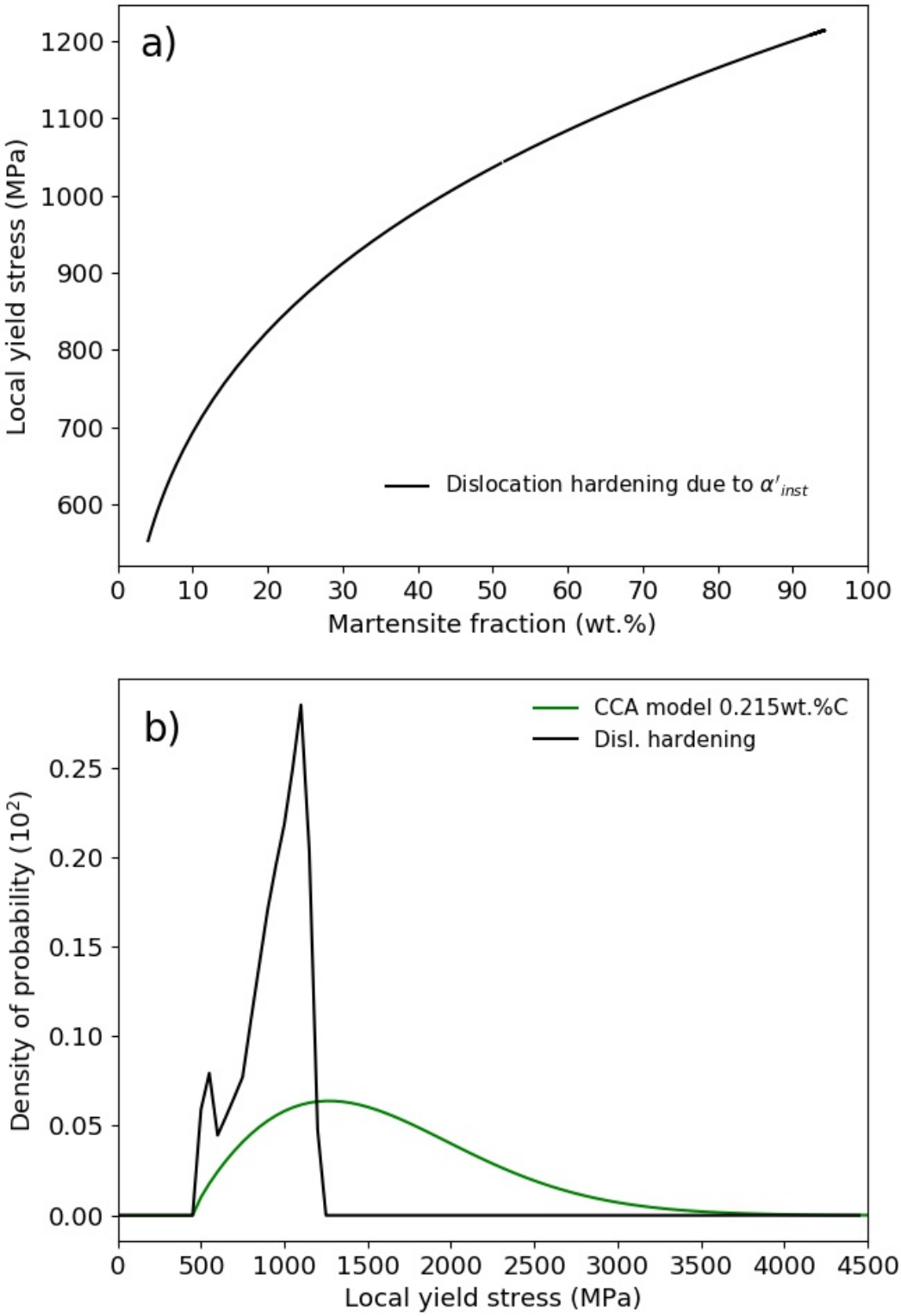

876

877 *Figure 11: a) The dislocation contribution to the yield stress for each newly formed martensite*
878 *fraction b) The density probability to find a lath with a given local yield stress considering only*
879 *the measured dislocation. These experimental values are compared to the expected stress*
880 *distribution necessary to explain the mechanical behavior of the studied steel according to* [2].